Effects of correlations on triplet loss processes in organic phosphorescent emission layers: Accurate and fast master equation modeling

M. Taherpour,* C. van Hoesel,* R. Coehoorn, and P. A. Bobbert†
Department of Applied Physics and Institute for Complex Molecular Systems, Eindhoven University of Technology, P. O. Box 513, NL-5600 MB Eindhoven, The Netherlands

(Received 5 January 2024; revised 5 March 2024; accepted 18 March 2024; published 3 April 2024)

Loss of triplet excitons by triplet-triplet annihilation (TTA) and triplet-polaron quenching (TPQ) is a major problem in modern organic light-emitting diodes with phosphorescent host-guest emission layers. Modeling of TTA and TPQ in these emission layers is therefore important. However, this modeling is complicated by positional correlations among the triplets and polarons. Kinetic Monte Carlo (KMC) simulations can account for these correlations, but are computationally expensive. In a previous paper [Taherpour *et al.*, Phys. Rev. B **105**, 085202 (2022)] we developed a master equation approach to modeling of TTA that accurately accounts for correlations, and is at the same time fast. In the present work, we extend the approach to include modeling of TPQ. We calculate the influence of TTA and TPQ on transient photoluminescence experiments and on steady-state emission efficiency, using KMC simulations as benchmark. We show that our extended master equation modeling is an accurate and fast alternative to KMC simulations.

DOI: 10.1103/PhysRevB.109.165202

I. INTRODUCTION

Excitonic processes are central to the functioning of organic optoelectronic devices, including organic light-emitting diodes (OLEDs). These processes involve a complex interplay of exciton radiative and nonradiative decay, diffusion, dissociation, and exciton quenching at high excitation densities due to exciton-exciton and exciton-charge interactions. In modern phosphorescent OLEDs, the loss of triplet excitons by triplet-triplet annihilation (TTA) and triplet-polaron quenching (TPQ) is the main reason for the efficiency roll-off with increasing current [1–6]. Efficient operation of phosphorescent OLEDs therefore relies on understanding and mitigating TTA and TPQ. We will in this work consider Förster-type TTA and TPQ processes. In the case of TTA, this means that the energy of a triplet exciton on a phosphorescent molecule is transferred by a virtual photon to a second phosphorescent molecule carrying a triplet exciton, bringing that molecule to an excited triplet state. The second molecule thermally relaxes back to the original unexcited triplet state, so that effectively the energy of the first triplet exciton is lost [7,8]. In the case of Förster-type TPQ, the virtual photon brings a second molecule carrying a polaron in an excited polaron state [9]. The excited polaron state relaxes thermally back to the original unexcited polaron state, after which the energy of the triplet is lost [10,11]. Charge imbalances in the emissive layer (EML), the presence of charge traps in the material, different electron and hole mobilities in the charge transport layers and the EML, and charge accumulation at the interfaces of the layers may substantially influence the quenching processes [12–15]. Due to the complex interplay of the various processes, it has been difficult to link the results of individual experiments to actual device performance. Modeling and simulating experimental roll-off curves to analyze the cause of the roll-off is therefore important [4,5].

Various efforts have been made using different modeling and simulation methods to describe TTA and TPQ and their effect on OLED performance. In time-resolved photoluminescence (TRPL) experiments, where triplet excitons in a phosphorescent emission layer are generated at time $t = 0$ by a short light flash, the decay of the time-dependent triplet volume density $T(t)$ is usually described by the phenomenological equation

$$\frac{dT}{dt} = -T/\tau - \frac{1}{2}k_{\mathrm{TTA}}T^2 - k_{\mathrm{TPQ}}TP, \tag{1}$$

where τ is the triplet lifetime, k_{TTA} and k_{TPQ} are TTA and TPQ rate coefficients, and P is the polaron volume density (we assume for simplicity no difference in quenching for electron and hole polarons). The problem with Eq. (1) is that it ignores spatial correlations in between the locations of triplets and between the locations of triplets and polarons. Taking into account such correlations is crucial for an accurate description of TRPL experiments [8,11,16]. Mechanistic kinetic Monte Carlo (KMC) simulations of TTA and TPQ automatically take into account correlations, but they come with high computational expenses [10]. For the case of TTA, we recently showed that a master equation (ME) approach, in which a hierarchical set of equations for triplet correlation functions of increasing order is approximately solved, provides an accurate and computationally competitive alternative to KMC simulations [17].

In this paper, we will extend the ME modeling approach of Ref. [17] to include also TPQ. Our approach, described in Sec. II B, starts by formulating the ME for the probabilities

*These authors contributed equally to this work.
†Corresponding author: p.a.bobbert@tue.nl

that the system of triplets and polarons is in a particular state. We then derive from this ME a Bogoliubov-Born-Green-Kirkwood-Yvon (BBGKY) hierarchy of equations for triplet-polaron distribution functions of increasing order. Following our previous work [17], we consider closures for the hierarchy by either neglecting correlations altogether, i.e., by making the mean-field approximation, or by taking into account correlations in the superposition approximation [18–21]. For TTA, the (SA) was found by us to be excellent at low and even at quite high triplet densities [17]. We will consider a phosphorescent emission layer consisting of molecules of a phosphorescent guest dispersed in a host molecular semiconductor. As a reference, we will also consider a pure phosphorescent layer. For definiteness, we will assume that both TTA and TPQ are long-range Förster-type processes. Triplet diffusion among the emitter molecules will also assumed to be a Förster-type process. We will describe polaron hopping by a Miller-Abrahams rate [22]. Extending our theory to other types of TTA, TPQ, triplet diffusion, and polaron hopping processes would be straightforward. We will take a constant polaron density and assume that triplets can only be generated on molecular sites that are not occupied by triplets or polarons.

The paper is structured as follows. In Sec. II, we explain the used methods. In Secs. II A and II B we explain the details of the KMC and ME methods, respectively. Some useful analytical expressions derived from the ME in limiting cases are given in the Appendix. Readers primarily interested in the results of the work can immediately go to Sec. III, where we present the results of our ME modeling using the mean-field (MF) approximation and the SA introduced in Sec. II B. The results are compared to KMC results, which serve as validation and benchmark. We consider both the transient case as occurring in a TRPL experiment and the steady-state case, where triplets are continuously generated, as occurring in a photoluminescence (PL) experiment with continuous illumination or in OLEDs under stationary operating conditions. We will not compare with actual experiments, but rather focus on the accuracy of the methods for a range of relevant cases. In Sec. IV, we consider the computational efficiency of our ME calculations using the SA as compared to KMC simulations. Finally, Sec. V contains a summary, conclusions, and an outlook.

II. METHODS

The system that we study represents an emission layer of a phosphorescent OLED. We model the layer as a cubic lattice of sites, representing molecules, with a lattice constant $a = 1$ nm, the typical intermolecular distance in molecular semiconductors. There is a fraction c_g of randomly positioned guest molecules. We assume that the energy difference between triplet excitons, triplets for short, on the host and the phosphorescent guest molecules is such that the triplets are only present on the guest molecules. TPQ can be classified into two categories based on whether the transport of (electron or hole) polarons is confined to the host or guest. For simplicity, we will ignore this confinement issue and assume that the polarons can be on the host as well as on the guest. For actual OLEDs, the guest concentration c_g is small (typically 10%). For the case of confinement of the polarons to the host, the influence of the presence of the guest on the polaron transport is then experimentally found to be small [23], justifying our assumption. For the case of a pure phosphorescent layer ($c_g = 100\%$), this confinement issue of course plays no role.

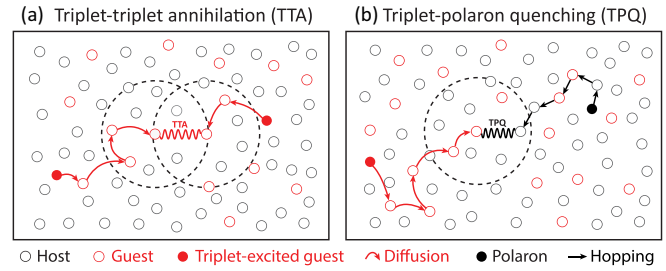

FIG. 1. Schematic overview of the main processes involved in (a) triplet-triplet annihilation (TTA) and (b) triplet-polaron quenching (TPQ) in a system of a phosphorescent guest emitter in a host molecular semiconductor. The dashed circles indicate the region within a Förster radius around triplets undergoing TTA or TPQ (wiggly lines). Both triplet diffusion and polaron hopping will enhance TTA and TPQ.

We neglect energetic disorder for triplets, so that there is no energy difference between triplets on different guest sites. Calculations for Ir-cored phosphorescent emitters yield an approximately Gaussian triplet energy disorder with a standard deviation of about 0.05 eV [24], which can be considered, at room temperature, as a weak disorder. We will not consider Coulomb interactions between the polarons. Coulomb interactions can become important at high polaron concentrations of about 10^{-2} per site [25,26] that we will not consider here. In the absence of Coulomb interactions, correlations in the positions of polarons play a very minor role [27,28] and these can therefore be neglected. Future extensions of the theory presented here could include Coulomb interactions giving rise to polaron-polaron correlations.

As shown in Fig. 1, the efficiency loss due to TTA and TPQ can be enhanced by triplet diffusion and polaron hopping. We will consider the following processes:

(1) Radiative decay of triplets on the guest sites with a rate $k_r = 1/\tau$. A typical value for the triplet lifetime of a phosphorescent emitter is $\tau = 1$ µs. We assume here for simplicity that the nonradiative decay rate is zero, so that k_r is the radiative decay rate. It is straightforward to extend the presented results to a nonzero nonradiative decay rate.

(2) Förster-type TTA, governed by a Förster radius $R_{F,TTA}$. The rate for TTA involving two triplets at sites i and j at a mutual distance r_{ij}, where the triplet at i is annihilated, is given by

$$S_{ij} = S(r_{ij}) = k_r \left(\frac{R_{F,TTA}}{r_{ij}} \right)^6 . \tag{2}$$

We note that $S_{ij} = S_{ji}$, so that the rate that quenching of one of the two triplets takes place is $2S_{ij}$.

(3) Förster-type TPQ, governed by a Förster radius $R_{F,TPQ}$. The rate for TPQ between a triplet at site i and a polaron at site j is given by

$$Q_{ij} = Q(r_{ij}) = k_r \left(\frac{R_{F,TPQ}}{r_{ij}} \right)^6 . \tag{3}$$

(4) Diffusion of triplets in between guest sites by Förster transfer with a Förster radius $R_{\mathrm{F,diff}}$. The rate for Förster transfer of a triplet at site i to an empty site j is given by

$$D_{ij} = D(r_{ij}) = k_{\mathrm{r}}\left(\frac{R_{\mathrm{F,diff}}}{r_{ij}}\right)^6. \tag{4}$$

In modeling of the roll-off curve of a phosphorescent white OLED with KMC simulations we found good agreement for $R_{\mathrm{F,TTA}} = R_{\mathrm{F,TPQ}} = 3$ nm, and $R_{\mathrm{F,diff}} = 1.5$ nm [4], which we consider as typical values.

(5) Polaron transport among host and guest sites by a hopping mechanism governed by the Miller-Abrahams (MA) hopping rate of a polaron between site i and an empty site j [22],

$$W_{ij} = \nu_1 \exp[-2(r_{ij}-a)/\lambda] \times \begin{cases} \exp\left(-\frac{\Delta E_{ij}}{k_{\mathrm{B}}T}\right), & E_j > E_i \\ 1, & E_j \leqslant E_i \end{cases}, \tag{5}$$

where ΔE_{ij} is the energy difference between sites i and j, r_{ij} is the intersite distance, ν_1 is the nearest-neighbor hopping prefactor, k_{B} is the Boltzmann constant, and T is the temperature. For the wave-function decay length we take $\lambda = 0.3$ nm, which was found to yield an excellent description of hole transport in the typical molecular semiconductor m-MTDATA used in an experimental study of TPQ by our group [23]. For this value, it is sufficient to consider hops up to a maximum distance $r_{ij} = 3$ nm. We take $\nu_1 = 3.34 \times 10^4/\tau$, which yields for a phosphorescent lifetime $\tau = 1$ µs a nearest-neighbor hopping frequency $\nu_1 = 3.34 \times 10^{10}$ s^{-1}. This rate is typical for molecular semiconductors [29] and comparable to the value $\nu_1 = 4.6 \times 10^{10}$ s^{-1} used in Ref. [23].

(6) Generation of triplets with a generation rate G at random emitter sites that are not already occupied by a triplet or a polaron. This generation can take place by illumination, such as in a PL experiment, or by recombination of electrons and holes.

We will consider two different situations, corresponding to two types of experiments. In the first situation, we start with a randomly generated configuration of triplets on guest sites and a thermal distribution of polarons on host or guest sites. We then study the density of triplets $T(t)$ as a function of time t. This situation is representative of a TRPL experiment, where a phosphorescent emission layer is illuminated by a short light pulse, after which the luminescence is measured as a function of time. We will assume that the polaron density is constant, so that the TRPL experiment corresponds to exciting a phosphorescent layer where a constant density of hole polarons is maintained by a current flow [23]. In the second situation, there is a constant generation rate G of triplets, and the steady-state density of triplets T as a function of G is studied. This would correspond to a phosphorescent emission layer of an OLED under constant operation conditions, where excitons are generated by a constant illumination or by electron-hole recombination. In both situations, we will assume that the electric field in the emission layer is small, so that we can neglect its effect on the polaron motion.

A. KMC simulations

Our benchmark results are obtained with KMC simulations [10], performed with the software tool BUMBLEBEE [30]. Simulation boxes of $100 \times 100 \times 100$ sites of a simple cubic lattice are used with periodic boundary conditions. We use cutoff distances of $2R_{\mathrm{F,TTA}}$, $2R_{\mathrm{F,TPQ}}$, and $2R_{\mathrm{F,diff}}$ for the TTA, TPQ, and triplet diffusion processes. We checked that taking larger cutoffs does not have a significant effect on the results. Since energy disorder is not taken into account for triplets, the TTA, TPQ, and triplet diffusion rates are symmetric: $S_{ij} = S_{ji}$, $Q_{ij} = Q_{ji}$, and $D_{ij} = D_{ji}$. We calculated the presented results from 100–300 simulation runs, depending on the required accuracy, for nominally equal systems with different disorder configurations. Error bars are shown on the data when relevant.

B. General theory

In Ref. [17] we developed a ME modeling approach for TTA with inclusion of triplet diffusion. To include TPQ, we need to extend that approach, because of the presence of two distinct species: triplets and polarons. We have N molecular lattice sites in the system, of which a fraction c_{g} are guest sites. At each site k we define a tuple $n_k = (n_k^{\mathrm{T}}, n_k^{\mathrm{P}})$, with $n_k^{\mathrm{T,P}} \in \{0, 1\}$. The tuple specifies if there is a triplet ($n_k = (1, 0)$) or a polaron ($n_k = (0, 1)$) on the site, or if the site is empty ($n_k = (0, 0)$). A particular state of the system is indicated as $\xi = (n_1, \ldots, n_N)$. The probability that the system is in this state at time t is $P_\xi(t) = P(n_1, \ldots, n_N; t)$. We can incorporate the above six processes into the ME,

$$\begin{aligned}
&\frac{dP(n_1,\ldots,n_N;t)}{dt} \\
&= \sum_{i,j,i\neq j} \big[-S_{ij} n_i^{\mathrm{T}} n_j^{\mathrm{T}} P(n_1,\ldots,n_N;t) \\
&\quad + S_{ij} n_i^{\mathrm{T}}\big(1-n_j^{\mathrm{T}}\big) P\big(n_1,\ldots,n_i^{\mathrm{T}},\ldots,n_j^{\mathrm{T}}+1,\ldots,n_N;t\big)\big] \\
&\quad + \sum_{i,j,i\neq j} \big[-Q_{ij} n_i^{\mathrm{P}} n_j^{\mathrm{T}} P\big(n_1,\ldots,n_i^{\mathrm{P}},n_j^{\mathrm{T}},\ldots,n_N\big) \\
&\quad + Q_{ij}\big(1-n_j^{\mathrm{T}}\big) n_i^{\mathrm{P}} P\big(n_1,\ldots,n_i^{\mathrm{P}},\ldots,n_j^{\mathrm{T}}+1,\ldots,n_N\big)\big] \\
&\quad + \sum_{i,j,i\neq j} \big[-D_{ij} n_i^{\mathrm{T}}\big(1-n_j^{\mathrm{T}}\big)\big(1-n_i^{\mathrm{P}}\big)\big(1-n_j^{\mathrm{P}}\big) \\
&\quad \times P(n_1,\ldots,n_N;t) + D_{ij} n_j^{\mathrm{T}}\big(1-n_i^{\mathrm{T}}\big)\big(1-n_i^{\mathrm{P}}\big)\big(1-n_j^{\mathrm{P}}\big) \\
&\quad \times P\big(n_1,\ldots,n_i^{\mathrm{T}}+1,n_j^{\mathrm{T}}-1,n_N;t\big)\big] \\
&\quad + \sum_{i,j,i\neq j} \big[-W_{ij} n_i^{\mathrm{P}}\big(1-n_j^{\mathrm{P}}\big)\big(1-n_j^{\mathrm{T}}\big)\big(1-n_i^{\mathrm{T}}\big) \\
&\quad \times P(n_1,\ldots,n_N;t) + W_{ij} n_j^{\mathrm{P}}\big(1-n_i^{\mathrm{P}}\big)\big(1-n_j^{\mathrm{T}}\big)\big(1-n_i^{\mathrm{T}}\big) \\
&\quad \times P\big(n_1,\ldots,n_i^{\mathrm{P}}+1,n_j^{\mathrm{P}}-1,n_N;t\big)\big] \\
&\quad + \sum_i \big[-k_{\mathrm{r}} n_i^{\mathrm{T}} P(n_1,\ldots,n_N;t) \\
&\quad + k_{\mathrm{r}}\big(1-n_i^{\mathrm{T}}\big) P\big(n_1,\ldots,n_i^{\mathrm{T}}+1,\ldots,n_N;t\big)\big] \\
&\quad + \sum_i \big[-G\big(1-n_i^{\mathrm{T}}\big)\big(1-n_i^{\mathrm{P}}\big) P(n_1,\ldots,n_N;t) \\
&\quad + G\big(1-n_i^{\mathrm{P}}\big) n_i^{\mathrm{T}} P\big(n_1,\ldots,n_i^{\mathrm{T}}-1,\ldots,n_N;t\big)\big],
\end{aligned} \tag{6}$$

where the terms with S_{ij}, Q_{ij}, D_{ij}, W_{ij}, k_r, and G describe TTA, TPQ, triplet diffusion, polaron diffusion, triplet radiative decay, and triplet generation, respectively. In order to simplify the notation, we only indicate the elements of the tuples that are involved in the process. For example, we write $P(n_1,\ldots,n_i^\mathrm{P},\ldots,n_j^\mathrm{T}+1,\ldots,n_N)$ instead of $P(n_1,\ldots,(n_i^\mathrm{T},n_i^\mathrm{P}),\ldots,(n_j^\mathrm{T}+1,n_j^\mathrm{P}),\ldots,n_N)$.

We define the one-site distribution function for polarons,

$$P_k^\mathrm{P}=\sum_\xi n_{k,\xi}^\mathrm{P}P_\xi(t), \tag{7}$$

and for triplets,

$$P_k^\mathrm{T}=\sum_\xi n_{k,\xi}^\mathrm{T}P_\xi(t), \tag{8}$$

where $n_{k,\xi}^\mathrm{P}$ is the polaron occupation number of site k (0 or 1) and $n_{k,\xi}^\mathrm{T}$ is the triplet occupation number of site k (0 or 1) in state ξ. From Eq. (6) in conjunction with Eqs. (7) and (8), we obtain the following equation for the one-site polaron distribution function:

$$\begin{aligned}\frac{dP_k^\mathrm{P}}{dt}=\sum_{l\neq k}\big[&-W_{kl}\big(P_k^\mathrm{P}-P_{kl}^\mathrm{PP}-P_{kl}^\mathrm{PT}\big)\\&+W_{lk}\big(P_l^\mathrm{P}-P_{kl}^\mathrm{PP}-P_{kl}^\mathrm{PT}\big)\big],\end{aligned} \tag{9}$$

and for the one-site triplet distribution function,

$$\begin{aligned}\frac{dP_k^\mathrm{T}}{dt}=&-k_rP_k^\mathrm{T}+G\big(1-P_k^\mathrm{T}-P_k^\mathrm{P}\big)\\&+\sum_{l\neq k}\big[D_{kl}\big(P_l^\mathrm{T}-P_k^\mathrm{T}\big)-Q_{kl}P_{kl}^\mathrm{TP}-S_{kl}P_{kl}^\mathrm{TT}\big],\end{aligned} \tag{10}$$

where P_{kl}^PP is the two-site polaron-polaron distribution function, P_{kl}^TT the two-site triplet-triplet distribution function, and P_{kl}^TP the two-site triplet-polaron distribution function. For the triplet-polaron distribution function

$$P_{kl}^\mathrm{TP}=\sum_\xi n_{k,\xi}^\mathrm{T}n_{l,\xi}^\mathrm{P}P_\xi(t), \tag{11}$$

we obtain from Eq. (6)

$$\begin{aligned}\frac{dP_{kl}^\mathrm{TP}}{dt}=&-k_\mathrm{r}P_{kl}^\mathrm{TP}-Q_{kl}P_{kl}^\mathrm{TP}+G\big(P_k^\mathrm{P}+P_l^\mathrm{P}-2P_{kl}^\mathrm{PP}-2P_{kl}^\mathrm{TP}\big)\\&-\sum_{m\neq k,l}\big[(S_{km}+S_{lm})P_{klm}^\mathrm{TPT}-(Q_{km}+Q_{lm})P_{klm}^\mathrm{TPP}\big]\\&+\sum_{m\neq k,l}\big[D_{km}\big(P_{lm}^\mathrm{PT}-P_{kl}^\mathrm{TP}\big)+D_{km}\big(P_{klm}^\mathrm{TPP}-P_{klm}^\mathrm{PPT}\big)\\&+D_{lm}\big(P_{km}^\mathrm{PT}-P_{kl}^\mathrm{PT}\big)+D_{lm}\big(P_{klm}^\mathrm{PTP}-P_{klm}^\mathrm{PPT}\big)\big]\\&+\sum_{m\neq k,l}\big[W_{km}\big(P_{km}^\mathrm{TP}-P_{kl}^\mathrm{TP}\big)+W_{km}\big(P_{klm}^\mathrm{PTT}-P_{klm}^\mathrm{TTP}\big)\\&+W_{lm}\big(P_{km}^\mathrm{TP}-P_{kl}^\mathrm{TP}\big)+W_{lm}\big(P_{klm}^\mathrm{TPT}-P_{klm}^\mathrm{TTP}\big)\big].\end{aligned} \tag{12}$$

Similarly, for the triplet-triplet distribution function

$$P_{kl}^\mathrm{TT}=\sum_\xi n_{k,\xi}^\mathrm{T}n_{l,\xi}^\mathrm{T}P_\xi(t), \tag{13}$$

we obtain

$$\begin{aligned}\frac{dP_{kl}^\mathrm{TT}}{dt}=&-2k_\mathrm{r}P_{kl}^\mathrm{TT}-2S_{kl}P_{kl}^\mathrm{TT}+G\big(P_k^\mathrm{T}+P_l^\mathrm{T}-2P_{kl}^\mathrm{TT}-2P_{kl}^\mathrm{PT}\big)\\&-\sum_{m\neq k,l}\big[(S_{km}+S_{lm})P_{klm}^\mathrm{TTT}-(Q_{km}+Q_{lm})P_{klm}^\mathrm{TTP}\big]\\&+\sum_{m\neq k,l}\big[D_{km}\big(P_{lm}^\mathrm{TT}-P_{kl}^\mathrm{TT}\big)+D_{km}\big(P_{klm}^\mathrm{TTP}-P_{klm}^\mathrm{PTT}\big)\\&+D_{lm}\big(P_{km}^\mathrm{TT}-P_{kl}^\mathrm{TT}\big)+D_{lm}\big(P_{klm}^\mathrm{TTP}-P_{klm}^\mathrm{TPT}\big)\big],\end{aligned} \tag{14}$$

and, lastly, for the polaron-polaron distribution function

$$P_{kl}^\mathrm{PP}=\sum_\xi n_{k,\xi}^\mathrm{P}n_{l,\xi}^\mathrm{P}P_\xi(t), \tag{15}$$

we obtain

$$\begin{aligned}\frac{dP_{kl}^\mathrm{PP}}{dt}=\sum_{m\neq k,l}\big[&W_{mk}\big(P_{ml}^\mathrm{PP}-P_{klm}^\mathrm{TPP}-P_{klm}^\mathrm{PPP}\big)\\&-W_{km}\big(P_{kl}^\mathrm{PP}-P_{klm}^\mathrm{PPT}-P_{klm}^\mathrm{PPP}\big)\\&+W_{ml}\big(P_{km}^\mathrm{PP}-P_{klm}^\mathrm{PTP}-P_{klm}^\mathrm{PPP}\big)\\&-W_{lm}\big(P_{kl}^\mathrm{PP}-P_{klm}^\mathrm{PPT}-P_{klm}^\mathrm{PPP}\big)\big].\end{aligned} \tag{16}$$

The above procedure could be continued in a straightforward way to distribution functions of increasingly higher order, generating a BBGKY hierarchy of equations [31–33]. However, higher-order distribution functions are not required for the purpose of this work, because of the specific closure that we will introduce.

As a first step towards defining the closure, we make the transition from distribution functions to correlation functions by introducing the two-site, or pair, correlation function as

$$g_{kl}^{\alpha\beta}=\frac{P_{kl}^{\alpha\beta}}{P_k^\alpha P_l^\beta}, \tag{17}$$

and the three-site correlation function as

$$g_{klm}^{\alpha\beta\gamma}=\frac{P_{klm}^{\alpha\beta\gamma}}{P_k^\alpha P_l^\beta P_m^\gamma}, \tag{18}$$

and so on, where $\alpha,\beta,\gamma\in\{\mathrm{T},\mathrm{P}\}$. It is straightforward to formulate the above BBGKY hierarchy of equations in terms of correlation functions of increasing order. In this notation, neglecting pair correlations corresponds to $g_{kl}^{\alpha\beta}=1$.

Secondly, we note that, as polarons are not lost nor generated, the total polaron density will stay constant. We will from now on neglect correlations between polarons, setting $P_{kl}^\mathrm{PP}=P_k^\mathrm{P}P_l^\mathrm{P}$, as this was shown to be a very good approximation in the absence of Coulomb interactions [27]. We then do not need Eqs. (9) and (16) for calculating the polaron density and the polaron-polaron distribution function.

We will further proceed along similar lines as in our earlier work on TTA [17]. If there would be no triplet diffusion or polaron hopping, all sites would be equivalent after performing an average over all possible distributions of the randomly positioned guest and host sites. We would then have perfect lattice symmetry. However, because diffusion of triplets can

only occur among guest sites, diffusion is a percolative process, where fast triplet diffusion can occur along percolating pathways of guest sites that happen to be close to each other. This percolative process cannot be fully addressed without sacrificing the lattice symmetry. Instead, we use the approach followed in Ref. [17] and replace the typical minimal distance over which triplet transfer can occur by $c_g^{-1/3}a$ instead of a. This approach was shown to lead to very accurate results in the case of TTA [17]. In the presence of energy disorder, also polaron transport becomes a percolative process [34]. We address this percolation problem by replacing the MA hopping rate Eq. (5) by

$$W_{ij} = W(r_{ij}) = c_{\text{eff}}\nu_1 \exp[-2(r_{ij}-a)/\lambda], \tag{19}$$

where $c_{\text{eff}} < 1$ is a parameter that takes into account in an effective way the influence of disorder on the polaron transport. With these adaptations, the lattice symmetry is preserved. Following Ref. [17], we also make an approximation where the lattice is replaced by a continuum with a cutoff distance $r_0 = 0.7929\,a$. This cutoff distance is determined such that the lattice sum of the Förster-type distance dependence r^{-6}, with the origin excluded, becomes equal to the volume integral, with a spherical region of radius r_0 around the origin excluded [17].

These approximations allow us to simplify the above equations, where two-site correlation functions now only depend on the distance r between the sites, and three-site correlation functions only depend on the vector $\mathbf{r}'$ from the first to second site and on the vector $\mathbf{r}'$ from the first to the third site. Furthermore, $T \equiv P_k^{\text{T}}/a^3$ and $P \equiv P_k^{\text{P}}/a^3$ become the site-independent triplet and polaron volume densities. Equation (10) then transforms into

$$\frac{dT}{dt} = G\left(\frac{1}{a^3} - T - P\right) - k_{\text{r}}T - 4\pi\int_{r_0}^{\infty}[S(r)T^2 g^{\text{TT}}(r,t) + Q(r)TPg^{\text{TP}}(r,t)]r^2\,dr. \tag{20}$$

Equation (14) transforms into

$$\begin{aligned}\frac{dg^{\text{TT}}(r,t)}{dt} &= -2S(r)g^{\text{TT}}(r,t) + \frac{2G}{Ta^3}(1-g^{\text{TT}}(r,t)) + \frac{2GP}{T}(g^{\text{TT}}(r,t)-g^{\text{TP}}(r,t)) \\ &- \int_{V\setminus\delta V_0\setminus\delta V_{\mathbf{r}}} d\mathbf{r}'\{Pg^{\text{TTP}}(\mathbf{r},\mathbf{r}',t)[Q(r')+Q(|\mathbf{r}'-\mathbf{r}|)] \\ &- Tg^{\text{TTT}}(\mathbf{r},\mathbf{r}',t)[S(r')+S(|\mathbf{r}'-\mathbf{r}|)]\} + 2g^{\text{TT}}(r,t) \\ &\times \int_{V\setminus\delta V_0} d\mathbf{r}'[TS(r')g^{\text{TT}}(r',t) + PQ(r')g^{\text{TP}}(r',t)] \\ &+ 2\frac{c_g}{a^3}\int_{V\setminus\delta\tilde{V}_0\setminus\delta V_r} d\mathbf{r}'D(r')[g^{\text{TT}}(|\mathbf{r}'-\mathbf{r}|,t) - g^{\text{TT}}(r',t)] \\ &+ 2P\int_{V\setminus\delta\tilde{V}_0\setminus\delta V_r} d\mathbf{r}'D(r')[g^{\text{TTP}}(\mathbf{r},\mathbf{r}',t) - g^{\text{PTT}}(\mathbf{r},\mathbf{r}',t)].\end{aligned} \tag{21}$$

Finally, Eq. (12) transforms into

$$\begin{aligned}\frac{dg^{\text{TP}}(r,t)}{dt} &= -Q(r)g^{\text{TP}}(r,t) + \frac{2G}{Ta^3}(1-Pa^3)(1-g^{\text{TP}}(r,t)) \\ &- \int_{V\setminus\delta V_0\setminus\delta V_{\mathbf{r}}} d\mathbf{r}'[Tg^{\text{TPT}}(\mathbf{r},\mathbf{r}',t)S(r') \\ &+ Pg^{\text{TPP}}(\mathbf{r},\mathbf{r}',t)Q(|\mathbf{r}'-\mathbf{r}|,t)] + g^{\text{TP}}(r,t) \\ &\times \int_{V\setminus\delta V_0\setminus\delta V_{\mathbf{r}}} d\mathbf{r}'[Tg^{\text{TT}}(r',t)S(r') + Pg^{\text{TP}}(r',t)Q(r')] \\ &+ \frac{c_g}{a^3}\int_{V\setminus\delta\tilde{V}_0\setminus\delta V_r} d\mathbf{r}'D(r')[g^{\text{TP}}(|\mathbf{r}'-\mathbf{r}|,t) - g^{\text{TP}}(r,t)] \\ &+ P\int_{V\setminus\delta\tilde{V}_0\setminus\delta V_r} d\mathbf{r}'D(r')[g^{\text{TPP}}(\mathbf{r},\mathbf{r}',t) - g^{\text{PPT}}(\mathbf{r},\mathbf{r}',t)] \\ &+ \frac{c_g}{a^3}\int_{V\setminus\delta\tilde{V}_0\setminus\delta V_r} d\mathbf{r}'W(r')[g^{\text{TP}}(|\mathbf{r}'-\mathbf{r}|,t) - g^{\text{TP}}(r,t)] \\ &+ T\int_{V\setminus\delta\tilde{V}_0\setminus\delta V_r} d\mathbf{r}'W(r')[g^{\text{PTT}}(\mathbf{r},\mathbf{r}',t) - g^{\text{TTP}}(\mathbf{r},\mathbf{r}',t)].\end{aligned} \tag{22}$$

Here, $\delta V_{\mathbf{r}}$ and $\delta\tilde{V}_{\mathbf{r}}$ are spherical regions with a radius r_0 and $\tilde{r}_0 \equiv c_g^{1/3}r_0$, respectively, around the point $\mathbf{r}$, and $\setminus\delta V_{\mathbf{r}}$ and $\setminus\delta\tilde{V}_{\mathbf{r}}$ indicate that these regions should be excluded from the volume integral. δV_0 and $\delta\tilde{V}_0$ are spherical regions around the origin.

We close the hierarchy of equations by using the SA [18–21], as in our previous work on the application of the ME approach to TTA [17]. The SA expresses three-site correlation function as a product of two-site correlation functions, yielding very accurate results in the case of TTA [17]. The use of the SA in the present case implies

$$g^{\alpha\beta\gamma}(\mathbf{r},\mathbf{r}',t) \approx g^{\alpha\beta}(r,t)g^{\alpha\gamma}(r',t)g^{\beta\gamma}(|\mathbf{r}'-\mathbf{r}|,t). \tag{23}$$

As we will see in Sec. III, this also leads to very accurate results when including TPQ. In general, Eqs. (20)–(22), using Eq. (23) as closure, should be solved numerically. We do this in a similar way as in Ref. [17]. We obtain transient results by setting $G = 0$ and solving the resulting equations numerically, where the integrals are evaluated using a spectral method. Steady-state results are obtained by accounting for the terms including G and solving the equations until no further change in time is observed.

In the MF approximation, correlations in between triplets and between triplets and polarons are ignored, so that

$$g^{\text{TT}}(r,t) = g^{\text{TP}}(r,t) = 1. \tag{24}$$

Equation (20) then becomes

$$\frac{dT}{dt} = G\left(\frac{1}{a^3} - T - P\right) - k_{\text{r}}T - \frac{1}{2}k_{\text{TTA}}T^2 - k_{\text{TPQ}}TP, \tag{25}$$

with $k_{\text{TTA}} = 8\pi k_{\text{r}}R_{\text{F,TTA}}^6/3r_0^3$ and $k_{\text{TPQ}} = 4\pi k_{\text{r}}R_{\text{F,TPQ}}^6/3r_0^3$. Apart from the first term, this equation is identical to Eq. (1), with $k_{\text{r}} = 1/\tau$. Equation (25) can be solved analytically,

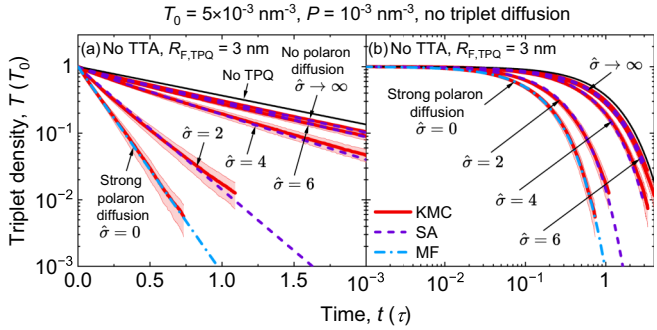

FIG. 2. Transient triplet density $T(t)$ in a simulation of a TRPL experiment in the absence of triplet diffusion and TTA with an initial triplet density $T_0 = 5 \times 10^{-3}$ nm^{-3}, polaron density $P = 10^{-3}$ nm^{-3}, and TPQ Förster radius $R_{F,TPQ} = 3$ nm. ME transients within the superposition approximation (SA) and mean-field (MF) approximation are given and compared to KMC results, for various values of $\hat{\sigma} \equiv \sigma/k_B T$. The transient for the case of no TPQ is also given. In (a) a linear and in (b) a logarithmic time axis is used. The pink area around the KMC results indicates the numerical uncertainty.

yielding

$$T(t) = \frac{1}{k_{TTA}} \left\{ k_2 \tanh\left(\tanh^{-1}\left(\frac{k_1 + k_{TTA} T_0}{k_2} \right) + \frac{1}{2} k_2 t \right) - k_1 \right\}, \tag{26}$$

where T_0 is the initial triplet density at $t = 0$, and where we have introduced $k_1 \equiv G + k_r + k_{TPQ} P$ and $k_2 \equiv \sqrt{(k_1)^2 + 2G k_{TTA}(1/a^3 - P)}$. The steady-state case is obtained in the limit $t \to \infty$ as $T = (k_2 - k_1)/k_{TTA}$, which gives T as a function of G.

As shown in the Appendix, in the limit of strong polaron diffusion and no triplet diffusion, and the limit of no triplet nor polaron diffusion, useful analytical results can be derived in the low triplet and low polaron-density approximation that go beyond the MF approximation.

III. RESULTS

A. Time-resolved photoluminescence—no triplet diffusion

In this subsection, we study how taking into account correlations affects the TRPL in the case of TPQ without and with TTA, assuming that there is no triplet diffusion. In a TRPL experiment, the triplets are initially distributed randomly. In the absence of triplet diffusion, the guest concentration becomes irrelevant, as the positions of the phosphorescent guest molecules are assumed to be random. This means that the results are applicable to host-guest systems with an arbitrary guest concentration. We compare ME results within the SA and the MF approximation to KMC results, which are our benchmark. The TRPL transients are given by the triplet density T as a function of time t, because the amount of triplets present at time t is proportional to the measured PL at that time. All our calculations and simulations are done at room temperature ($T = 295$ K).

Figure 2 shows TRPL transients $T(t)$ for an initial triplet density $T_0 = 5 \times 10^{-3}$ nm^{-3} and a polaron density $P = 10^{-3}$ nm^{-3}, without TTA, for $R_{F,TPQ} = 3.0$ nm and different values of $\hat{\sigma} \equiv \sigma/k_B T$, which is the dimensionless energy disorder strength for a Gaussian energy disorder with standard deviation σ at temperature T. As a reference, we include the result $T(t) = T_0 \exp(-k_r t)$ for the case that there is no TPQ. Fig. 2(b) shows the same results as Fig. 2(a), but with a logarithmic time axis. For a typical phosphorescent guest concentration of 10%, the chosen value $T_0 = 5 \times 10^{-3}$ nm^{-3} corresponds to 5% initial occupation of the guest molecules by a triplet. We see in the figure that the effect of TPQ becomes stronger when $\hat{\sigma}$ decreases, because the polarons then diffuse faster. For $\hat{\sigma} = 0$ polaron diffusion is so strong that correlations are washed out. As a consequence, the MF result Eq. (26), with $R_{F,TTA} = 0$, agrees excellently with the KMC result. The case $\hat{\sigma} = 0$ might not be realistic for the organic semiconductors used in OLEDs, but we remark that the strong polaron diffusion case can also occur for a nonzero $\hat{\sigma}$ when the nearest-neighbor hopping prefactor ν_1 in Eq. (5) is much larger than the value we assumed.

When polaron diffusion is not strong, the spatial correlation between triplets and polarons becomes important and the MF approximation breaks down. The neglect of correlations in the MF approximation leads to an overestimation of TPQ and, therefore, to an underestimated triplet density $T(t)$. For $\hat{\sigma} \to \infty$ there is no polaron diffusion, because all the polarons are trapped at energetically low-lying sites. We see that in that case the SA excellently describes the transient. The analytical result Eq. (A9) for $R_{F,TTA} = 0$ essentially coincides with the SA in this case (not shown). For intermediate values of $\hat{\sigma}$, c_{eff} in Eq. (19) has been adjusted to fit the KMC data. The fitted values of c_{eff} are given in Table I for $R_{F,TPQ} = 3$ nm and $P = 10^{-3}$ nm^{-3}. We also give in this table the corresponding polaron mobilities μ, as calculated from KMC simulations at vanishing electric field, and the polaron diffusion coefficient D, as obtained from μ via the generalized Einstein relation [35]. We note that the values of c_{eff} are not simply related to the polaron mobility or diffusion coefficient, because these are bulk properties that are only valid beyond a characteristic length scale L_0 of several nanometers, because of percolation effects [36]. By contrast, the parameter c_{eff} takes into account the effect on TPQ of the diffusion of polarons on a nanometer length scale relevant to the TPQ process. Thus, different values for c_{eff} are obtained for different $R_{F,TPQ}$. Table II shows in addition the values of c_{eff} for $R_{F,TPQ} = 2$ and 4 nm. For the highest disorder strength $\hat{\sigma} = 6$, c_{eff} is the same for the three different $R_{F,TPQ}$, which we attribute to the fact that the characteristic length scale is for $\hat{\sigma} = 6$ from Ref. [36] found to be $L_0 \approx 4.8$ nm. We then have $R_{F,TPQ} < L_0$ for all three values of $R_{F,TPQ}$ and can expect that for all three values of $R_{F,TPQ}$ the character of the TPQ process is the same. The c_{eff} values in Table I will be used in the remainder of this work, where we take $R_{F,TPQ} = 3$ nm. A dimensionless disorder strength $\hat{\sigma} = 4$, corresponding to $\sigma = 0.1$ eV at room temperature, is typical [23].

Figure 3 shows transients for $R_{F,TPQ} = 3.0$ nm, an initial triplet density $T_0 = 5 \times 10^{-3}$ nm^{-3} and different polaron densities P from 10^{-4} to 5×10^{-3} nm^{-3}, in the absence of triplet diffusion, polaron diffusion, and TTA. With increasing polaron density, the decay in $T(t)$ due to TPQ increases, leading to a nonexponential decay caused by the build-up of correlations between polarons and triplets, with a depletion zone

TABLE I. Values of c_{eff} in Eq. (19) used in the transients of Fig. 2 for $R_{\text{F,TPQ}} = 3$ nm, $P = 10^{-3}$ nm^{-3}, and various values of $\hat{\sigma}$. Also the corresponding polaron mobilities μ and diffusion coefficients D at vanishing electric field are given.

$\hat{\sigma} \equiv \sigma/k_{\text{B}}T$	c_{eff}	Mobility, μ [m^2/Vs]	Diffusion coefficient, D [m^2/s]
0	1	1.27×10^{-6}	3.29×10^{-8}
2	1.7×10^{-2}	8.47×10^{-8}	2.08×10^{-9}
4	1.1×10^{-3}	1.39×10^{-9}	2.52×10^{-11}
6	1.9×10^{-4}	1.95×10^{-11}	2.53×10^{-13}
∞	0	0	0

of triplets in the neighborhood of polarons. The figure shows thus clearly that in the case of weak or no polaron diffusion, a rate equation description of the efficiency loss due to TPQ [Eq. (1)] is not applicable. The magnification in Fig. 3(b) shows that for all polaron densities the SA transients perfectly follow the KMC transients, demonstrating that correlation effects are adequately taken into account. The transients are in this case also excellently described by Eq. (A9) for $R_{\text{F,TTA}} = 0$ (not shown).

B. Steady state—no triplet diffusion

We now consider the steady-state situation in which triplets are generated at a rate G at positions where there is no polaron or other triplet. This corresponds to a continuous illumination experiment or a situation in which triplets are generated at random positions by electron-hole recombination.

In Fig. 4, we show the steady-state triplet density T as a function of the generation rate G for (a) $\hat{\sigma} = 4$ and (b) $\hat{\sigma} \to \infty$ (no polaron diffusion), for the SA and MF approximations in comparison to KMC results. For $\hat{\sigma} = 4$ the value of c_{eff} from Table I was taken. Results are shown for the TPQ-only case with $R_{\text{F, TPQ}} = 3.0$ nm and the case of TPQ and TTA with $R_{\text{F, TPQ}} = R_{\text{F, TTA}} = 3.0$ nm. The boxes indicate three regimes. In regime I, TTA is insignificant, and almost all triplet loss is caused by TPQ and radiative decay. In the middle regime II, both TTA and TPQ contribute to the triplet loss. In regime III, TTA dominates over TPQ, and both SA and KMC results start to approach the TTA-only case indicated by the green line. As can be seen in Fig. 4(b) in comparison to Fig. 4(a), by increasing $\hat{\sigma}$ from 4 to $\hat{\sigma} \to \infty$ (when polarons do not diffuse anymore), regime II shifts to smaller G. This is because TPQ decreases with decreasing polaron diffusion and, therefore, TTA starts to dominate TPQ at lower generation rates. In contrast to the case of only TTA (green line), the results with TPQ do not approach the no-loss processes limit $T = G\tau a^{-3}/(1 + G\tau)$ (dotted line) for low G. This is because for very low generation rates TPQ is still significant. The MF results underestimate the triplet density by almost an order of magnitude, and in none of the three regimes the MF approximation is accurate. As can be seen in both Figs. 4(a) and 4(b) , the SA results are in excellent agreement with the benchmark KMC results. For the case $\hat{\sigma} \to \infty$ the T-G curves are also excellently described by the analytical result Eq. (A12) (not shown).

In Fig. 5 we show for $R_{\text{F,TPQ}} = R_{\text{F,TTA}} = 3.0$ nm and $\hat{\sigma} \to \infty$, $\hat{\sigma} = 4$, and $\hat{\sigma} = 0$ the steady-state triplet density T as a function of the generation rate G for polaron densities of (a) $P = 10^{-3}$ nm^{-3} and (b) $P = 5 \times 10^{-3}$ nm^{-3}. For the cases $\hat{\sigma} \to \infty$ and $\hat{\sigma} = 4$, the SA results accurately follow the KMC results. For the case $\hat{\sigma} = 0$, polaron hopping events occur so frequently in the KMC simulations as compared to other events that obtaining converged KMC results would take an unreasonable amount of CPU time. Therefore, no results are shown for this case. Nevertheless, also for this case we expect accurate agreement. In the case of $P = 10^{-3}$ nm^{-3} [Fig. 5(a)], TPQ is weak for $\hat{\sigma} \to \infty$ and $\hat{\sigma} = 4$, as can be seen from the approach to the no-loss processes limit (dotted line) at low G. For $\hat{\sigma} = 0$ polaron diffusion is strong enough to make TPQ significant. In the case of $P = 5 \times 10^{-3}$ nm^{-3} [Fig. 5(b)], TPQ is significant for all three values of $\hat{\sigma}$. At very high G, all results converge to the same curve, because TTA then dominates over TPQ, so that the polaron density and the diffusion speed of polarons become irrelevant. The SA results for $\hat{\sigma} = 0$ and $\hat{\sigma} \to \infty$ essentially coincide with the analytical results Eqs. (A6) and (A12), respectively, both for $P = 10^{-3}$ and 5×10^{-3} nm^{-3} (not shown).

TABLE II. Values of c_{eff} for different $R_{\text{F,TPQ}}$ at polaron density $P = 10^{-3}$ nm^{-3}.

$\hat{\sigma} \equiv \sigma/k_{\text{B}}T$	$R_{\text{F,TPQ}} = 2$ nm	$R_{\text{F,TPQ}} = 3$ nm	$R_{\text{F,TPQ}} = 4$ nm
0	1	1	1
2	3.1×10^{-3}	1.7×10^{-2}	4.5×10^{-2}
4	3.1×10^{-4}	1.1×10^{-3}	2.3×10^{-3}
6	1.9×10^{-4}	1.9×10^{-4}	1.9×10^{-4}
∞	0	0	0

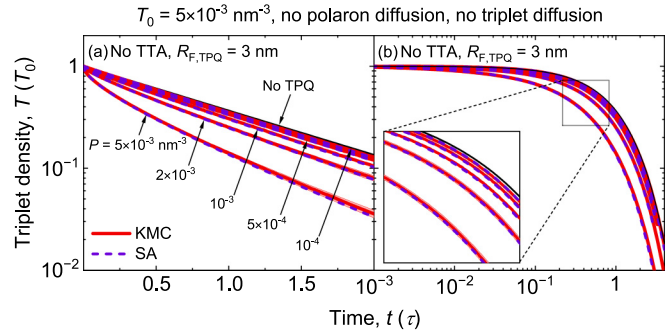

FIG. 3. Transient triplet density for $R_{\text{F,TPQ}} = 3$ nm, initial triplet density $T_0 = 5 \times 10^{-3}$ nm^{-3}, and different polaron densities P, in the absence of triplet diffusion, TTA, and polaron diffusion ($\hat{\sigma} \to \infty$). In (a) a linear and in (b) a logarithmic time axis is used. The inset in (b) is a magnification of the indicated region.

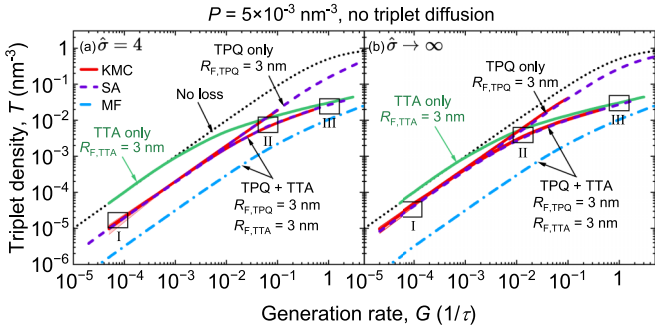

FIG. 4. Dependence of the steady-state triplet density T on the triplet generation rate G, for the TPQ-only case with $R_{\mathrm{F,\,TPQ}} = 3$ nm and the case of TPQ and TTA with $R_{\mathrm{F,\,TPQ}} = R_{\mathrm{F,\,TTA}} = 3$ nm, in the absence of triplet diffusion, for (a) $\hat{\sigma} = 4$ and (b) $\hat{\sigma} \to \infty$. The polaron density is $P = 5 \times 10^{-3}$ nm^{-3}. In regime I, TPQ dominates. In regime II, both TPQ and TTA are important. In regime III, TTA dominates. The green lines show the SA TTA-only results from our previous work [17]. The dotted lines show the no-loss processes limit.

Figure 6(a) shows for $R_{\mathrm{F,TPQ}} = R_{\mathrm{F,TTA}} = 3.0$ nm, $G\tau = 5 \times 10^{-4}$, and no polaron nor triplet diffusion SA and KMC results for the triplet-polaron pair correlation functions $g^{\mathrm{TP}}(r)$ for polaron densities $P \to 0$, $P = 10^{-3}$, and $P = 5 \times 10^{-3}$ nm^{-3}. For $P \to 0$ we only show the SA result. The SA yields a very good description of the pair correlation function as compared to KMC for $P = 10^{-3}$ nm^{-3}. For $P = 5 \times 10^{-3}$ nm^{-3} the SA slightly underestimates the correlation, resulting in a small underestimation of the steady-state triplet density, as seen in Fig. 5(b). The analytical result Eq. (A10) for $g^{\mathrm{TP}}(r)$ (not shown) essentially coincides with the SA results, because the triplet density and the polaron density are sufficiently small to make the low density-limit valid for both.

Figure 6(b) shows the triplet-polaron and triplet-triplet pair correlation functions $g^{\mathrm{TP}}(r)$ and $g^{\mathrm{TT}}(r)$, respectively, for $P = 5 \times 10^{-3}$ nm^{-3}, and $G\tau = 5 \times 10^{-3}$ and 5×10^{-2}. For these cases the SA describes the KMC pair correlation functions fairly well. The analytical results Eqs. (A10) and (A11) for $g^{\mathrm{TP}}(r)$ and $g^{\mathrm{TT}}(r)$, respectively, are given by the dotted green lines. In this case, deviations are seen from the SA results, because for the chosen values of G the triplet density is no longer very small. For the chosen value of P, Eqs. (A10) and (A11) almost give the same results, because $P \ll 1/a^3$, so that $g^{\mathrm{TP}}(r)$ and $g^{\mathrm{TT}}(r)$ are indistinguishable. The SA correctly predicts that $g^{\mathrm{TT}}(r)$ is actually slightly larger than $g^{\mathrm{TP}}(r)$.

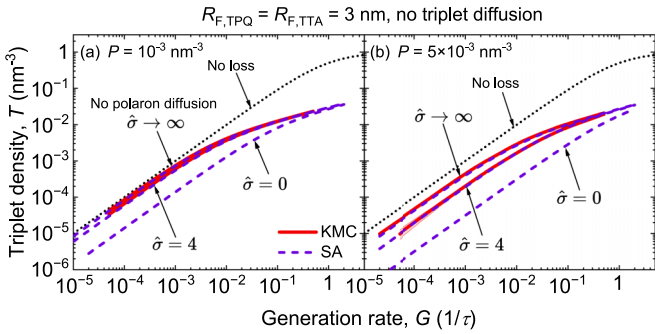

FIG. 5. Dependence of the steady-state triplet density T on the triplet generation rate G in the absence of triplet diffusion, for $R_{\mathrm{F,\,TPQ}} = R_{\mathrm{F,\,TTA}} = 3$ nm, for polaron densities (a) $P = 10^{-3}$ nm^{-3} and (b) $P = 5 \times 10^{-3}$ nm^{-3}, and three values of $\hat{\sigma}$.

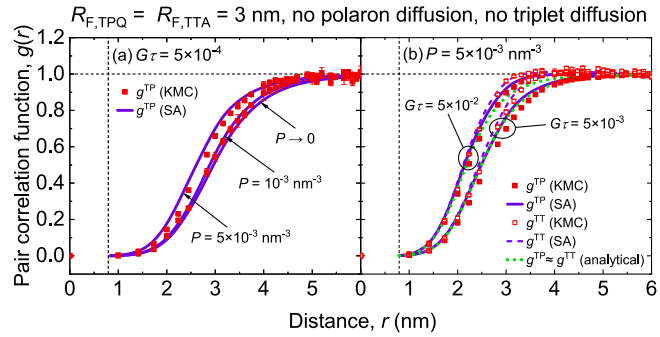

FIG. 6. Steady-state pair correlation functions $g(r)$ for $R_{\mathrm{F,TPQ}} = R_{\mathrm{F,TTA}} = 3$ nm and no polaron nor triplet diffusion. (a) Triplet-polaron correlation functions $g^{\mathrm{TP}}(r)$ for different polaron densities P. (b) Triplet-polaron correlation functions $g^{\mathrm{TP}}(r)$ and triplet-triplet correlation functions $g^{\mathrm{TT}}(r)$ for $P = 5 \times 10^{-3}$ nm^{-3} and two values of $G\tau$. KMC data points have discrete values of r, which are the distances from the origin in a cubic lattice with lattice constant $a = 1$ nm. The analytical results for $g^{\mathrm{TP}}(r)$ and $g^{\mathrm{TT}}(r)$ in (b) are given by Eqs. (A10) and (A11), respectively. The SA correlation functions are only defined for $r < r_0 = 0.7929$ nm (vertical dashed line). All correlation functions approach 1 for large r (horizontal dashed line).

C. Inclusion of triplet diffusion

In this subsection, we consider the effects of triplet diffusion on transient and steady-state triplet densities in the presence of TTA and TPQ. Because triplets can only diffuse among phosphorescent guests, it is now important to distinguish between guest sites, on which the triplets can reside, and host sites, which we assume to be inaccessible to triplets. We apply the approach explained in Sec. II B to account for the resulting percolative effects in an approximate way within the SA.

Figure 7 shows, for $R_{\mathrm{F,TPQ}} = 3.0$ nm, $R_{\mathrm{F,diff}} = 1.5$ nm, an initial triplet density $T_0 = 5 \times 10^{-3}$ nm^{-3}, guest concentration $c_{\mathrm{g}} = 100\%$, and various values of $\hat{\sigma}$, the transient triplet density $T(t)$ for the case without TTA [Figs. 7(a) and 7(b)] and TTA with $R_{\mathrm{F,TTA}} = 3.0$ nm Figs. 7(c) and 7(d)]. The insets in Figs. 7(b) and 7(d) show the excellent agreement of the SA with the KMC results, despite the fact that the energetic disorder is treated in an effective way by Eq. (19), taking the c_{eff} values from Table I. For the strong polaron diffusion case without TTA in panel (a) ($\hat{\sigma} = 0$), the MF approximation is again accurate because triplet-polaron correlations are washed out ($g^{\mathrm{TP}}(r) \to 1$). However, Fig. 7(c) shows that in the presence of TTA, the MF approximation is no longer accurate for strong polaron diffusion. The reason is that the triplet-polaron correlations are washed out by the strong polaron diffusion, but the triplet-triplet correlations not. As a result, the MF approximation overestimates the TTA. In Fig. 8 we show results for $R_{\mathrm{F,TPQ}} = 3.0$ nm, $R_{\mathrm{F,diff}} = 1.5$ nm, $T_0 = 5 \times 10^{-3}$ nm^{-3}, and $\hat{\sigma} \to \infty$ (no polaron diffusion). In Fig. 8(a) we show the transient triplet density $T(t)$ for the case

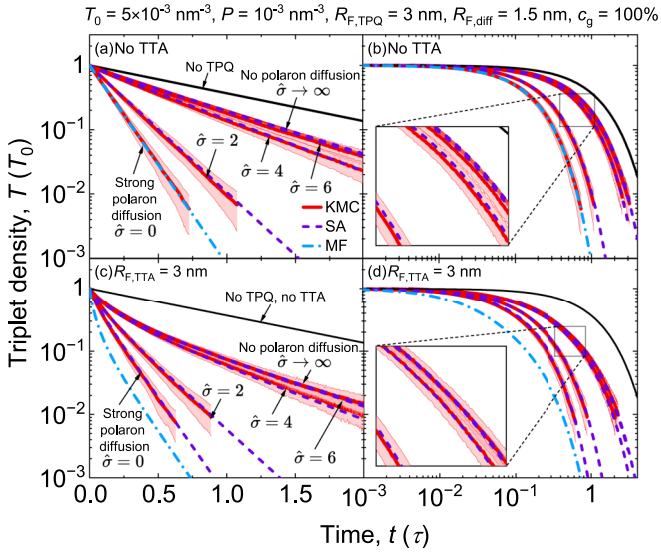

FIG. 7. Transient triplet density $T(t)$ for an initial triplet density $T_0 = 5 \times 10^{-3}$ nm^{-3}, a polaron density $P = 10^{-3}$ nm^{-3}, $R_{F,TPQ} = 3$ nm, in the presence of triplet diffusion with $R_{F,diff} = 1.5$ nm, and a guest concentration $c_g = 100\%$. (a) Transients without TTA for different values of $\hat{\sigma}$. (b) Same as (a), but with a logarithmic time axis. (c) and (d): same as (a) and (b), but including TTA with $R_{F,TTA} = 3$ nm. The insets in (b) and (d) are magnifications of the indicated regions. Numerical uncertainties are indicated by pink areas surrounding the KMC results.

without TTA, for a guest concentration $c_g = 100\%$ and various polaron densities, and in Fig. 8(b) for a polaron density $P = 5 \times 10^{-3}$ nm^{-3}, and c_g of 100% and 10%. Figures 8(c)

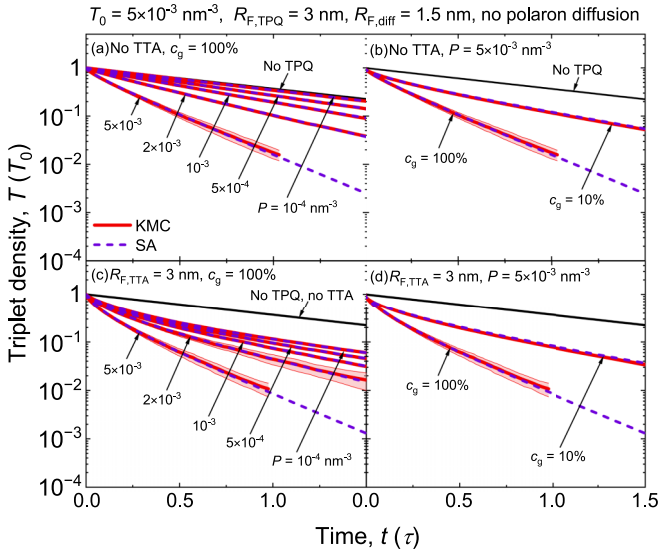

FIG. 8. Transient triplet density $T(t)$ for an initial triplet density $T_0 = 5 \times 10^{-3}$ nm^{-3}, $R_{F,TPQ} = 3.0$ nm, and no polaron diffusion ($\hat{\sigma} \to \infty$) in the presence of triplet diffusion with $R_{F,diff} = 1.5$ nm. (a) Transients for a guest concentration $c_g = 100\%$ and different polaron densities P, for the case without TTA. (b) Transients for $c_g = 10\%$ and 100%, and $P = 5 \times 10^{-3}$ nm^{-3}. (c) and (d): same as (a) and (b), but including TTA with $R_{F,TTA} = 3$ nm.

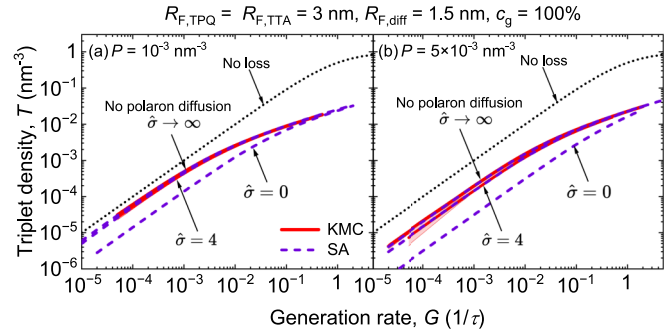

FIG. 9. Dependence of the steady-state triplet density T on the triplet generation rate G for $R_{F,TPQ} = R_{F,TTA} = 3$ nm in the presence of triplet diffusion with $R_{F,diff} = 1.5$ nm, and $c_g = 100\%$, for polaron densities (a) $P = 10^{-3}$ nm^{-3} and (b) $P = 5 \times 10^{-3}$ nm^{-3}, and three values of $\hat{\sigma}$. The dotted line shows the no-loss processes limit.

and 8(d) show similar results as (a) and (b), but including TTA with $R_{F,TTA} = 3.0$ nm. Figures 8(a) and 8(c) show that the change in the transients with increasing polaron density is excellently captured by the SA. Figures 8(b) and 8(d) show that for a realistic guest concentration $c_g = 10\%$ the change in transient by the dilution is also very well captured, despite the approximate approach of including percolation effects in the triplet diffusion, as explained in Sec. II B. We attribute the slight underestimation of triplet quenching by the SA for $c_g = 10\%$ to the slight underestimation of triplet diffusion by our approximate approach. In Figs. 9(a) and 9(b), the steady-state triplet density T is shown as a function of the generation rate G for $R_{F,TPQ} = R_{F,TTA} = 3.0$ nm, in the presence of triplet diffusion with $R_{F,diff} = 1.5$ nm, and $c_g = 100\%$, for polaron densities $P = 10^{-3}$ and 5×10^{-3} nm^{-3}, respectively, and for three different values of $\hat{\sigma}$. For $\hat{\sigma} \to \infty$ and $\hat{\sigma} = 4$, the SA results accurately follow the KMC results. For the same reasons as explained in the previous subsection, no converged KMC results could be obtained for $\hat{\sigma} = 0$. We see in Fig. 9(a) that the results for $\hat{\sigma} \to \infty$ and $\hat{\sigma} = 4$ almost coincide. We conclude from this that for a polaron density $P \leqslant 10^{-3}$ nm^{-3} and $\hat{\sigma} = 4$, typical for OLED materials, polaron diffusion does not need to be included in evaluating the steady-state triplet density in the presence of triplet diffusion. By comparing Fig. 9(a) to Fig. 9(b), we see that when increasing the polaron density to $P = 5 \times 10^{-3}$ nm^{-3}, polaron diffusion starts to become important for $\hat{\sigma} = 4$. Like in Fig. 5 we see that at very high G all results converge to the same curve, because TTA then dominates over TPQ. A comparison of the steady-state triplet density of the SA and the MF approximation with KMC results as a function of the generation rate for $R_{F,TPQ} = 3.0$ nm, $P = 10^{-3}$ and 5×10^{-3} nm^{-3}, $c_g = 100\%$, triplet diffusion with $R_{F,diff} = 1.5$ nm, and no polaron diffusion is shown in Fig. 10. Results are displayed for the cases without TTA in Figs. 10(a) and 10(b) and inclusion of TTA with $R_{F,TTA} = 3.0$ nm in Figs. 10(c) and 10(d). We see that for low G, triplet diffusion is not strong enough to wash out the correlations. As a result, the MF result is very inaccurate. Increasing the polaron density from $P = 10^{-3}$ to 5×10^{-3} nm^{-3} shows a noticeable decrease in the steady-state triplet density due to increasing TPQ and the MF results at low G become even more inaccurate. For increasing G, the MF results become gradually

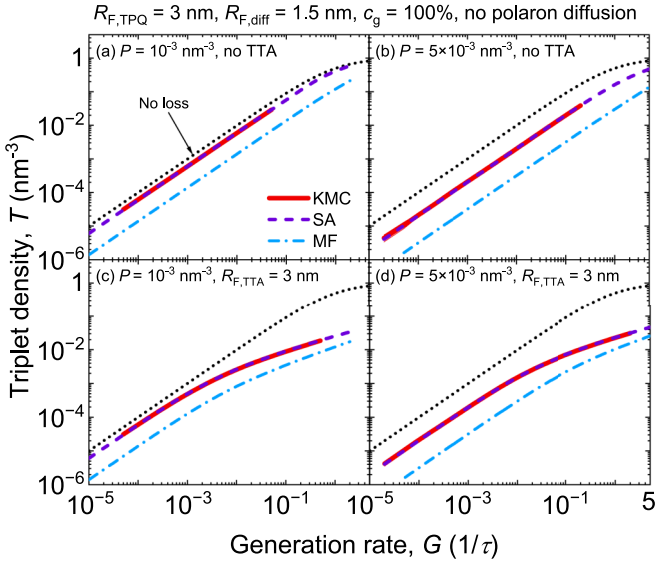

FIG. 10. Dependence of the steady-state triplet density T on the triplet generation rate for $R_{F,TPQ} = 3$ nm, $c_g = 100\%$, no polaron diffusion ($\hat{\sigma} \to \infty$), and $R_{F,diff} = 1.5$ nm, for (a) $P = 10^{-3}$ nm^{-3} and no TTA, and (b) $P = 5 \times 10^{-3}$ nm^{-3} and no TTA. (c) and (d) same as (a) and (b), but including TTA with $R_{F,TTA} = 3.0$ nm.

more accurate because correlations are getting washed out by the frequent generation of triplets at random positions. In all cases, the SA results are very accurate.

Steady-state results for the triplet density T as a function of the generation rate G for $\hat{\sigma} \to \infty$, $R_{F,TPQ} = R_{F,TTA} = 3.0$, $R_{F,diff} = 1.5$, and for $c_g = 100\%$ and 10% are shown in Fig. 11(a), and corresponding triplet-polaron correlation functions $g^{TP}(r)$ for $G\tau = 5 \times 10^{-3}$ in Fig. 11(b). The SA results for the steady-state triplet density are in very good agreement with the KMC results. For $c_g = 100\%$ there is also a good agreement for $g^{TP}(r)$, while the agreement is fair for $c_g = 10\%$. Figure 11(a) shows for $c_g = 10\%$ a small underestimation of the triplet density of the SA in comparison to KMC, which we attribute to our approximate way of including percolation effects in the triplet diffusion. This underestimation is in line with the slightly higher $g^{TP}(r)$ of the SA for $r > 3$ nm observed in Fig. 11(b).

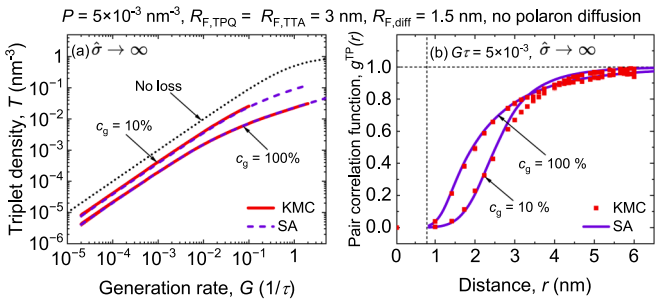

FIG. 11. (a) Dependence of the steady-state triplet density T on the triplet generation rate G, for $R_{F,TPQ} = R_{F,TTA} = 3$ nm, $R_{F,diff} = 1.5$ nm, no polaron diffusion ($\hat{\sigma} \to \infty$), and guest concentrations $c_g = 100\%$ and 10%. (b) Correlation functions corresponding to the results shown in (a) for $G\tau = 5 \times 10^{-3}$.

IV. COMPUTATIONAL EFFICIENCY

In this section, we compare the computational efficiency of ME calculations using the SA to that of KMC simulations. We focus on a comparison of the transient calculations. In the case of steady-state calculations, the comparison is not straightforward because of the different procedures used to reach the steady state. The ME calculations and KMC simulations were performed on comparable hardware (Intel Xeon Gold 6240 or comparable processors) with comparable numerical precision. The ME calculations were done with Python codes that can be further optimized and possibly, to some extent, parallelized. The KMC simulations were done with the highly optimized commercial software tool BUMBLEBEE [30].

As a first example, we consider TPQ with a Förster radius $R_{F,TPQ} = 3.0$ nm, no TTA, and no triplet diffusion. For the SA calculations, the CPU time is independent of the initial triplet density T_0 and the polaron density P, as is expected, whereas the CPU time increases steeply with increasing T_0 and P for the KMC simulations. For a typical polaron density $P = 10^{-3}$ nm^{-3}, an initial triplet density $T_0 = 5 \times 10^{-3}$ nm^{-3}, and a dimensionless disorder strength $\hat{\sigma} = 4$, the KMC simulations take for a single run about a factor of 30 longer than the SA calculations. The transient KMC results for this case, presented in Sec. III A, were obtained by averaging over 100 runs. The SA calculations, which require only a single run, were in this case at least three orders of magnitude more CPU time-efficient than the KMC simulations.

As a second example, we consider the case $P = 10^{-3}$ nm^{-3}, $T_0 = 5 \times 10^{-3}$ nm^{-3}, $R_{F,TPQ} = R_{F,TTA} = 3.0$ nm, including triplet diffusion with $R_{F,diff} = 1.5$ nm, and different guest concentrations c_g. The CPU time for the SA calculations is almost independent of c_g. For the KMC simulations, the CPU time increases approximately linearly with c_g. For a guest concentration of $c_g = 100\%$, the KMC simulations take for a single run about a factor 20 longer than the SA calculations for $\hat{\sigma} = 4$. By decreasing the value of $\hat{\sigma}$ to 2 and 0, the gain factor increases to 80 and 300, respectively. The KMC simulations for this case, presented in Sec. III C, are averaged over a typical number of 100 runs and take at least three orders of magnitude longer than the SA calculations.

Parallel execution of KMC simulation runs for various disorder configurations can significantly reduce the wall time as compared to the CPU time for examples mentioned above. For example, in the case of 100 individual runs, the reduction in wall time can be two orders of magnitude. However, the speed of the ME code can also be further increased by optimization and parallelization.

V. SUMMARY, CONCLUSIONS, AND OUTLOOK

We developed and applied a new master equation (ME) modeling method to the description of Förster-type triplet-triplet annihilation (TTA) and triplet-polaron quenching (TPQ), including polaron hopping and Förster-type triplet diffusion. The method is applicable to organic emission layers consisting of a guest phosphorescent emitter embedded in a host molecular semiconductor. From the ME, a hierarchical chain of equations was derived that includes the correlations in the positions of the triplets and polarons to increasing

order. Following our previous work on TTA [17], we solved this chain of equations by approximating three-site correlation functions as products of two-site correlation function using the superposition approximation (SA). We found that the SA yields very accurate results for relevant quantities, as benchmarked by kinetic Monte Carlo (KMC) simulations. This holds both for transient situations corresponding to time-resolved photoluminescence (TRPL) experiments as well as for steady-state situations. The CPU time required for the SA calculations is in some cases orders of magnitude less than for the KMC simulations, which makes this type of modeling an attractive alternative. In addition, this type of modeling provides important insights into the role of correlations in the TTA and TPQ processes.

Extensions of this work could involve other than Förster-type TTA, TPQ, and diffusion, like their short-range Dexter-type versions, and other, more realistic, types of polaron hopping rates. When Coulomb interactions between the polarons are taken into account, polaron-polaron correlations become important and should be included at high polaron densities. In the present work, approximations were made to preserve the lattice symmetry, in conjunction with a continuum approximation, so that two-site correlation functions only depend on the distance between the sites. In principle, these approximations do not need to be made. Without these approximations, the solution of the involved equations will be technically more difficult, but possibly still feasible. Percolative effects in the triplet and polaron motion can then be explicitly accounted for.

ACKNOWLEDGMENTS

This publication is part of the project "Master Equation Modeling of Organic Light-Emitting Diodes" (MEMOLED), with Project No. 17120, of the research programme "High Tech Systems and Materials" of the Netherlands Organization for Scientific Research (NWO). The project is jointly financed by NWO and Simbeyond B.V.

The master equation calculations were performed by M.T., with a computer program developed by Cv.H. The kinetic Monte Carlo simulations were performed by M.T. The analytical expressions in the Appendix were derived by Cv.H. The theoretical master equation framework was developed jointly by M.T. and Cv.H. All authors contributed to the writing of the manuscript. The work was supervised by P.A.B. and R.C.

APPENDIX: ANALYTICAL SOLUTIONS FOR LIMITING CASES

Analytical solutions of Eqs. (20)–(22) can be obtained in the limiting cases of (i) strong polaron diffusion and no triplet diffusion, and (ii) no triplet nor polaron diffusion [37]. We additionally apply a low triplet and low polaron-density approximation. Because we neglect correlations in between polarons, we have $g^{\mathrm{PP}}(r,t)=1$. Furthermore, all correlations vanish for large distances,

$$\lim_{r\to\infty} g^{\alpha\beta}(r,t)=1. \tag{A1}$$

In the transient cases that we will consider, no correlations are initially present at $t=0$ so that

$$g^{\alpha\beta}(r,0)=1, \tag{A2}$$

in accordance with the physical initial conditions of a TRPL experiment.

(i) In the case of strong polaron diffusion ($W(r)\to\infty$) and no triplet diffusion, the strong polaron diffusion washes out the correlations between polarons and triplets, so that $g^{\mathrm{TP}}(r,t)=1$. For this case, we separately consider the transient solution, to be compared with a TRPL experiment, and the steady-state solution. For the transient solution ($G=0$) in the regime of low triplet and polaron density, the first term on the right-hand side of Eq. (21) is dominant and $g^{\mathrm{TT}}(r,t)$ is obtained as

$$g^{\mathrm{TT}}(r,t)=e^{-2S(r)t}. \tag{A3}$$

With this, the solution of Eq. (20) becomes

$$T(t)=T_0e^{-k_3t}\left(1+\frac{\sqrt{2}\,T_0\pi^2R_{\mathrm{F,TTA}}^3}{3\sqrt{k_3/k_{\mathrm{r}}}}\,\mathrm{erf}(\sqrt{k_3t})\right)^{-1}, \tag{A4}$$

where $k_3\equiv k_{\mathrm{r}}+k_{\mathrm{TPQ}}P$. Here, we have additionally assumed that $r_0\ll R_{\mathrm{F,TTA}}$, so that the integral of the first term in square brackets of Eq. (20) can be extended to $r=0$. This is a good approximation for a typical value $R_{\mathrm{F,TTA}}=3$ nm.

For the steady-state case, we derive an expression for $g^{\mathrm{TT}}(r)$ by taking into account additionally the terms proportional to G at the right-hand side of Eq. (21) and putting the time derivative on the left-hand side equal to zero,

$$g^{\mathrm{TT}}(r)=\frac{1}{1+\frac{TS(r)}{G\left(\frac{1}{a^3}-P\right)}}. \tag{A5}$$

By substituting this expression into Eq. (20) and setting dT/dt equal to zero, we obtain as equation for the steady-state solution

$$-k_1T+G\left(\frac{1}{a^3}-P\right)-\frac{2\pi^2}{3}a^{3/2}T^{3/2}\sqrt{Gk_{\mathrm{r}}(1-Pa^3)}\times\left(\frac{R_{\mathrm{F,TTA}}}{a}\right)^3=0. \tag{A6}$$

From this equation, T can be solved as a function of G. Here, we have again assumed that the integral of the first term in square brackets in Eq. (20) can be extended to $r=0$.

(ii) In the limit of no triplet nor polaron diffusion, we can also obtain exact results when both the triplet and polaron densities are low. In the transient case, we find again that $g^{\mathrm{TT}}(r,t)$ is given by

$$g^{\mathrm{TT}}(r,t)=e^{-2S(r)t}. \tag{A7}$$

We obtain $g^{\mathrm{TP}}(r,t)$ from Eq. (22) by again taking into account only the first term on the right-hand side, yielding

$$g^{\mathrm{TP}}(r,t)=e^{-Q(r)t}. \tag{A8}$$

Substituting the expressions for $g^{\mathrm{TT}}(r,t)$ and $g^{\mathrm{TP}}(r,t)$ into Eq. (20) yields as a solution

$$T(t) = T_0 e^{-\left(k_r + 2k_4 Pa^3/\sqrt{k_r t}\right)t}\left(1 + \frac{\sqrt{2}}{3} T_0 \pi^2 R_{\mathrm{F,TTA}}^3 e^{\left(k_4 Pa^3/k_r\right)^2} \times \left[\mathrm{erf}\left(k_4 Pa^3/k_r + \sqrt{k_r t}\right) - \mathrm{erf}\left(k_4 Pa^3/k_r\right)\right]\right)^{-1}, \tag{A9}$$

where $k_4 \equiv (2/3)k_r \pi^{3/2} R_{\mathrm{F,TPQ}}^3/a^3$. In this case the integrals of both terms in square brackets in Eq. (20) have been extended to $r = 0$, which now requires both $r_0 \ll R_{\mathrm{F,TTA}}$ and $r_0 \ll R_{\mathrm{F,TPQ}}$.

To obtain the steady-state solution, we solve Eq. (22) in the low triplet and low polaron-density approximation, which yields, after putting the left-hand side equal to zero,

$$g^{\mathrm{TP}}(r) = \frac{1}{1 + \frac{TQ(r)}{G\left(\frac{1}{a^3} - P\right)}}. \tag{A10}$$

Next, this solution is employed to solve Eq. (21) in the low triplet and low polaron-density approximation, resulting in

$$g^{\mathrm{TT}}(r) = \frac{G\left(\frac{1}{a^3} - P g^{\mathrm{TP}}(r)\right)}{G\left(\frac{1}{a^3} - P\right) + TS(r)}. \tag{A11}$$

Finally, by substituting these expressions for $g^{\mathrm{TP}}(r)$ and $g^{\mathrm{TT}}(r)$ into Eq. (20), we obtain

$$G(1 - Pa^3) = Ta^3(G + k_r) + \frac{2}{3}\pi^2 P R_{\mathrm{F,TPQ}}^3 \sqrt{G k_r T a^3 (1 - Pa^3)} + \frac{2}{3}\pi^2 \sqrt{\frac{G k_r T^3 a^3}{1 - Pa^3}} R_{\mathrm{F,TTA}}^3 \times \left(1 - Pa^3 \frac{R_{\mathrm{F,TTA}}^3}{R_{\mathrm{F,TTA}}^3 + R_{\mathrm{F,TPQ}}^3}\right). \tag{A12}$$

The steady-state triplet density can be found by solving this equation for T as a function of G.

[1] C. Adachi, M. A. Baldo, S. R. Forrest, and M. E. Thompson, High-efficiency organic electrophosphorescent devices with tris (2-phenylpyridine) iridium doped into electron-transporting materials, Appl. Phys. Lett. **77**, 904 (2000).

[2] M. A. Baldo, C. Adachi, and S. R. Forrest, Transient analysis of organic electrophosphorescence. II. Transient analysis of triplet-triplet annihilation, Phys. Rev. B **62**, 10967 (2000).

[3] C. Murawski, K. Leo, and M. C. Gather, Efficiency roll-off in organic light-emitting diodes, Adv. Mater. **25**, 6801 (2013).

[4] M. Mesta, H. van Eersel, R. Coehoorn, and P. A. Bobbert, Kinetic Monte Carlo modeling of the efficiency roll-off in a multilayer white organic light-emitting device, Appl. Phys. Lett. **108**, 133301 (2016).

[5] H. van Eersel, P. A. Bobbert, R. A. J. Janssen, and R. Coehoorn, Monte Carlo study of efficiency roll-off of phosphorescent organic light-emitting diodes: Evidence for dominant role of triplet-polaron quenching, Appl. Phys. Lett. **105**, 143303 (2014).

[6] S. Wehrmeister, L. Jäger, T. Wehlus, A. F. Rausch, T. C. G. Reusch, T. D. Schmidt, and W. Brütting, Combined electrical and optical analysis of the efficiency roll-off in phosphorescent organic light-emitting diodes, Phys. Rev. Appl. **3**, 024008 (2015).

[7] S. Reineke, K. Walzer, and K. Leo, Triplet-exciton quenching in organic phosphorescent light-emitting diodes with Ir-based emitters, Phys. Rev. B **75**, 125328 (2007).

[8] H. van Eersel, P. A. Bobbert, and R. Coehoorn, Kinetic Monte Carlo study of triplet-triplet annihilation in organic phosphorescent emitters, J. Appl. Phys. **117**, 115502 (2015).

[9] R. H. Young, J. R. Lenhard, D. Y. Kondakov, and T. K. Hatwar, 47.2: Luminescence quenching in blue fluorescent OLEDs, SID Symp. Dig. Tech. Pap. **39**, 705 (2008).

[10] H. van Eersel, P. A. Bobbert, R. A. J. Janssen, and R. Coehoorn, Effect of Förster-mediated triplet-polaron quenching and triplet-triplet annihilation on the efficiency roll-off of organic light-emitting diodes, J. Appl. Phys. **119**, 163102 (2016).

[11] R. Coehoorn, P. A. Bobbert, and H. van Eersel, Förster-type triplet-polaron quenching in disordered organic semiconductors, Phys. Rev. B **96**, 184203 (2017).

[12] D. Hertel and K. Meerholz, Triplet-polaron quenching in conjugated polymers, J. Phys. Chem. B **111**, 12075 (2007).

[13] J. Lee, J.-I. Lee, J.-W. Lee, and H. Y. Chu, Effects of charge balance on device performances in deep blue phosphorescent organic light-emitting diodes, Org. Electron. **11**, 1159 (2010).

[14] S. Reineke, G. Schwartz, K. Walzer, and K. Leo, Reduced efficiency roll-off in phosphorescent organic light emitting diodes by suppression of triplet-triplet annihilation, Appl. Phys. Lett. **91**, 123508 (2007).

[15] B. Diouf, W. S. Jeon, R. Pode, and J. H. Kwon, Efficiency control in iridium complex-based phosphorescent light-emitting diodes, Adv. Mater. Sci. Eng. **2012**, 794674 (2012).

[16] R. Coehoorn, P. A. Bobbert, and H. van Eersel, Effect of exciton diffusion on the triplet-triplet annihilation rate in organic semiconductor host-guest systems, Phys. Rev. B **99**, 024201 (2019).

[17] M. Taherpour, C. van Hoesel, R. Coehoorn, and P. A. Bobbert, Accurate and fast master equation modeling of triplet-triplet annihilation in organic phosphorescent emission layers including correlations, Phys. Rev. B **105**, 085202 (2022).

[18] J. G. Kirkwood, Statistical mechanics of fluid mixtures, J. Chem. Phys. **3**, 300 (1935).

[19] J. G. Kirkwood and E. M. Boggs, The radial distribution function in liquids, J. Chem. Phys. **10**, 394 (1942).

[20] L. Monchick, J. Magee, and A. Samuel, Theory of radiation chemistry. IV. Chemical reactions in the general track composed of *N* particles, J. Chem. Phys. **26**, 935 (1957).

[21] T. Waite, Theoretical treatment of the kinetics of diffusion-limited reactions, Phys. Rev. **107**, 463 (1957).

[22] A. Miller and E. Abrahams, Impurity conduction at low concentrations, Phys. Rev. **120**, 745 (1960).

[23] A. Ligthart, T. D. Nevels, C. H. Weijtens, P. A. Bobbert, and R. Coehoorn, Mechanistic description of the efficiency loss in organic phosphorescent host–guest systems due to triplet-polaron quenching, Org. Electron. **91**, 106058 (2021).

[24] X. de Vries, P. Friederich, W. Wenzel, R. Coehoorn, and P. A. Bobbert, Triplet exciton diffusion in metalorganic phosphorescent host-guest systems from first principles, Phys. Rev. B **99**, 205201 (2019).

[25] J. Zhou, Y. C. Zhou, J. M. Zhao, C. Q. Wu, X. M. Ding, and X. Y. Hou, Carrier density dependence of mobility in organic solids: A Monte Carlo simulation, Phys. Rev. B **75**, 153201 (2007).

[26] F. Liu, H. van Eersel, B. Xu, J. G. E. Wilbers, M. P. de Jong, W. G. van der Wiel, P. A. Bobbert, and R. Coehoorn, Effect of Coulomb correlation on charge transport in disordered organic semiconductors, Phys. Rev. B **96**, 205203 (2017).

[27] J. Cottaar and P. A. Bobbert, Calculating charge-carrier mobilities in disordered semiconducting polymers: Mean field and beyond, Phys. Rev. B **74**, 115204 (2006).

[28] A. V. Shumilin and Y. M. Beltukov, System of correlation kinetic equations and the generalized equivalent circuit for hopping transport, Phys. Rev. B **100**, 014202 (2019).

[29] S. L. M. van Mensfoort, V. Shabro, R. J. de Vries, R. A. J. Janssen, and R. Coehoorn, Hole transport in the organic small molecule material α-NPD: evidence for the presence of correlated disorder, J. Appl. Phys. **107**, 113710 (2010).

[30] https://simbeyond.com, the Bumblebee software is provided by Simbeyond B.V.

[31] N. N. Bogoliubov, Kinetic equations, J. Phys. USSR **10**, 265 (1946).

[32] M. Born and H. S. Green, A general kinetic theory of liquids I. The molecular distribution functions, Proc. R. Soc. London A **188**, 10 (1946).

[33] E. M. Lifshitz and L. P. Pitaevskii, *Physical Kinetics* (Butterworth Heinemann, Oxford, 1981).

[34] J. Cottaar, L. J. A. Koster, R. Coehoorn, and P. A. Bobbert, Scaling theory for percolative charge transport in disordered molecular semiconductors, Phys. Rev. Lett. **107**, 136601 (2011).

[35] Y. Roichman, Y. Preezant, and N. Tessler, Analysis and modeling of organic devices, Phys. Status Solidi (a) **201**, 1246 (2004).

[36] A. Massé, R. Coehoorn, and P. A. Bobbert, Universal size-dependent conductance fluctuations in disordered organic semiconductors, Phys. Rev. Lett. **113**, 116604 (2014).

[37] C. van Hoesel, Master equation modeling of excitonic loss processes in phosphorescent OLEDs: On the importance of spatial correlations, MSc thesis, Eindhoven University of Technology, 2021.